Journal of Fluids and Structures 59 (2015) 270–284

Contents lists available at ScienceDirect

Journal of Fluids and Structures

journal homepage: www.elsevier.com/locate/jfs

Nonlinear network modeling of multi-module floating structures with arbitrary flexible connections

H.C. Zhang [a], D.L. Xu [a,*], S.Y. Xia [a], C. Lu [a], E.R. Qi [b], C. Tian [b], Y.S. Wu [b]

[a] State Key Laboratory of Advanced Design and Manufacturing for Vehicle Body, Hunan University, Changsha 410082, PR China
[b] China Ship Scientific Research Center, Wuxi 214082, PR China

ARTICLE INFO

Article history:
Received 30 March 2015
Accepted 24 September 2015

Keywords:
Floating structure
Network dynamics
Flexible connector
Nonlinear dynamics

ABSTRACT

Multiple floating modules connected by flexible connectors can be viewed as a network structure. A standard modeling process for multi-module floating structures in arbitrary topology is presented by using network theory. A three-dimensional model is developed using the linear wave theory, dynamic model of single floating module, constitutive model of flexible connectors and model of a mooring system. As a typical application, a floating airport model is established and further its nonlinear dynamic responses and connector loads are analyzed. Numerical results show that the traditional linear analysis may underestimate the actual results. The methodology applied in this paper is extensible to many engineering problems with network structures alike.

1. Introduction

The needs for ocean space utilization are expected to be increasing in future according to the rapid expansion of modern industrial cities among coastal areas. Surely, very large floating structure (VLFS), which could be utilized as a floating airport, mobile offshore base, floating pier, floating plant, floating city, floating storage facility, etc., plays a great role of the utilization of ocean space because it has various merits in view points of economy, safety, and environmental friendliness (Park et al., 2004). In order to perform its various functions and meet the constraints of safety and cost, intensive efforts should be made in the initial conceptual design stage, structural arrangements, construction process and maintenance after operation (Lee and Newman, 2000; Rognaas et al., 2001; Utsunomiya et al., 2004).

Among the various fields of design technology for VLFS, it is no doubt that the safety design of floating structures based on hydrodynamic response analysis is one of the most important concerns (Du and Ertekin, 1991) particularly for some applications that require stringent tolerance on the deformation of the floating structure. For example, the maximum pitch angle between modules is less than about 0.86° for the aircraft operation on Mobile Offshore Base in Sea State 6(Rognaas et al., 2001). In the past decades, the research on VLFS involves two types of floating bodies, the box shaped pontoon type and the semi-submersible type. The hydroelastic theory has been widely applied to analyze the dynamics characteristics (Price and Wu, 1986) due to the small draft in comparison with its length for the pontoon type VLFS. The common approach is to model the entire floating structure by a single beam or plate based on the classical thin plate theory while the water wave is modeled by using the linear wave theory (Aoki, 1997; Hamamoto, 1994; Kashiwagi, 1998; Khabakhpasheva and Korobkin,

* Correspondence to: College of Mechanical and Vehicle Engineering, Hunan University, Yuelu District, Changsha City, Hunan Province, PR China. Tel.: +86 731 88821791; fax: +86 731 88822051.
E-mail address: dlxu@hnu.edu.cn (D.L. Xu).

http://dx.doi.org/10.1016/j.jfluidstructs.2015.09.012
0889-9746/

2001). For the larger draft to length ratios as opposed to the mat-like VLFS, this necessitates to model the floating structure as a thick plate by using Mindlin plate theory (Watanabe et al., 2006). The floating structures discussed above are all viewed as a single continuum structure and their responses are obtained by using the linearized modal superposition or finite element discretization method. Due to its vast scale of VLFS, a single continuum structure may cause extreme high deformation loads in the internal of the structure and may also be troublesome in construction, transportation and deployment. Thus multiple standardized modules with flexible connectors are concerned (Watanabe et al., 2004) where the connection plays an important role in dynamic responses. Maeda et al. (1979) studied the one-dimensional behavior of floating structures consisting of rigid modules with rigid or pin connectors for regular waves by a strip method. Fu et al. (2007) and Wang et al. (2009) proposed the use of hinge or semi-rigid connectors instead of rigid ones since the non-rigid connectors are more effective in reducing the hydroelastic response as comparing to the rigid connectors. Khabakhpasheva and Korobkin (2002) and Xia et al. (2000) dealt with a VLFS as two-dimensional articulated beams or plates connected by idealized connectors that are considered as two independent vertical and rotational springs. They showed that the hydroelastic response is strongly dependent on the stiffness of connectors and the incoming wave frequency. Gao et al. (2011) examined the effects of the location and the rotational stiffness of a flexible line connection on the hydroelastic response. A pontoon type floating structure (PFS) which consists of deformable floating modules connected with flexible connectors in longitudinal and (or) transverse directions is studied by Michailides et al. (2013). The effect of the connector's rotational stiffness and the grid type of the PFS on the hydroelastic response and the connectors' internal load are analyzed. The results indicated a complicated relationship between the internal load of the connectors and the hydroelastic response of the examined PFS configurations when examining the effects of the connectors' rotational stiffness and the excitation for the grid type PFS. The semi-submersible type floating structure is an optimal choice in order to reduce the hydrodynamic response in the deep sea area. To determine its hydroelastic response, it requires a structural model of VLFS considering the elasticity of the structure, and a hydrodynamic model for the fluid force. Kim et al. (1999) developed a three-dimensional hydroelastic model of a multi-module linked floating structure under regular waves with arbitrary angle by using FEM for structures and WIMIT program for the fluid where the connector is represented by a linearized stiffness matrix with respect to the displacements at the module connection points. However, the analysis for a refined finite element model is hardly executed due to the massive scale of the floating structure. Thus there is motivation to use rigid modules, flexible connector (RMFC) model (Wang et al., 1991), especially for conceptual and preliminary design. In the RMFC model, the VLFS is represented by multiple rigid modules connected by flexible connectors with assigned stiffness properties (Riggs and Ertekin, 1993). The connectors are usually modeled as simple linear and 'zero-length' springs (Riggs et al., 1998a). Paulling and Tyagi (1993) introduced a RMFC model with four modules in which each module was modeled by slender tubular members using the Morison formula and a pair of modules are connected by a combination of springs and damping devices (dashpots) to generate linear proportional forces. A comparative study of the linear wave induced response of a 5-module mobile offshore base (MOB) on two structural models (rigid module with flexible connector model and finite element shell model) is reported in Riggs et al.'s works (2000). The results showed that the simplified RMFC model can predict the response very well if the parameters correspond well to the FEM model's. Reviewing the recent research works above and many others not listed here carefully, we can conclude that almost all of the modeling methods adopt the linearization approach for the classical beam (or plate) model or FEM models for VLFS. When dealing with connector models, it is common to assume the flexible connection as independent linear springs in all degrees of freedom or discretized stiffness matrix using FEM method. This treatment ignores the effect of nonlinearity and artificially decouples the interaction of the module motions through connection points. Due to the large scale of floating modules, small motions of the floating modules may lead to large displacements at the connection points so that it could give rise to strong geometrical non-linearities in the connector model even if the connector element possesses linear elasticity characteristics. The nonlinearity may induce a variety of complex dynamic behaviors, very different from the linear results such as response jumping, motion synchronization and phase lock among the floating modules (Xu et al., 2014a; Zhang et al., 2015a). As for topological forms, VLFS may be constructed in diverse platform shapes, such as chain-type for a floating runway (June Bai et al., 2001), rectangular-type for entertainment facilities (Koh and Lim, 2009), circular-type for an artificial island (Andrianov and Hermans, 2005). In fact, there have been few modeling works to deal with various topology structures for VLFS.

A multi-module floating structure connected by flexible connectors in a particular topology is a typical network structure where each module under the excitation of waves can be viewed as an oscillator and a connector is viewed as a coupling between the oscillators. The dynamic network theory can be utilized to model and predict the nonlinear dynamics of VLFS. Our preliminary research on two dimensional problems of a chain-type floating airport (Xu et al., 2014a, 2014b; Zhang et al., 2015a, 2015b) confirms the feasibility of the new methodology for such applications. This method showed that the non-linear effect could significantly influence the dynamics prediction of the floating airport in which complex dynamical behaviors have been investigated, including sudden changes of module responses and connector loads (Xu et al., 2014a), the amplitude death phenomena for the global dynamic stability (Xu et al., 2014b), collectively synergistic effect of network dynamics among floating modules due to coupling (Zhang et al., 2015a). These works are the initial attempt of introducing nonlinear network dynamics theory to floating airport in marine engineering to enrich the methodology in the prediction of dynamics response of VLFS.

This paper presents a new approach for modeling three dimensional problems of VLFS in arbitrary structure topology, while the previous works (Xu et al., 2014a, 2014b; Zhang et al., 2015a) are only limited to two dimensional problems (surge, heave and pitch motions) with a chain-type platform. With the three dimensional model to be developed, one enables to

perform the dynamic prediction of any shaped VLFS on directional sea. In this paper, a standard modeling process for multi-module floating structure with any configuration of connectors will be elaborated. A generalized network model of the multi-module floating structure is developed based on the linear wave theory, a dynamic model of single floating module, a constitutive model of the connector and model of a mooring system. An application example of a chain-type floating airport is illustrated. Nonlinear dynamic responses and connector loads of the floating airport are numerically analyzed together with the linear results to indicate the significant difference from the nonlinear scenario. The feasibility of the modeling method introduced in this paper is not limited to the chain-type floating airport and theoretically suitable for all kinds of VLFS with complex topology network structures.

2. Network modeling of multi-module floating structures with flexible connectors

Multiple floating modules coupled by flexible connectors can be viewed as a network structure. In this section, a generalized network model for VLFS with arbitrary topology form is developed, by integrating the hydrodynamic model of a single floating module and model of connector, and model of mooring system constraints, where the topologic structure form is defined by a topology connection matrix of the floating structure.

2.1. Preliminaries

Before the derivation of the mathematical model, we need to define coordinate references, number the floating modules and construct the topology matrix.

First we set up two coordinate references. One is the global coordinate (x, y, z), also referred as Earth-fixed reference, of which the $x-y$-axis plan coincides with the water free surface and the z-axis points upwards. The other is local coordinate (ζ_i, η_i, ξ_i), corresponding to Body-fixed reference of the i-th module. The rotation center of the resting floating module is defined as origin of the local coordinate, $\zeta_i - \eta_i$ axes are parallel with undisturbed free-surface and ξ_i axis points upwards. A sketch of the coordinates is shown in Fig. 1.

Next, we should number every module of the floating system. The rule of numbering is that the difference between the two assigned numbers of adjacent modules is the least. By so doing the topology matrix to be developed appears to be diagonal and compacted.

For the general purpose of describing any topological form of VLFS, such as chain-type, rectangular-type or circular-type, in the model, a connection topology matrix $\Phi \in \mathbb{R}^{N\times N}$ is introduced to deal with arbitrary topological structures. A schematic diagram for the construction of topology matrix for N numbers of floating modules is shown in Fig. 2. The rows and columns of the topology matrix indicate the numbering of modules and its element Φ_{ij} is set to 1 as long as the i-th module connects with the j-th module, otherwise Φ_{ij} is set to zero. The diagonal element Φ_{ii} is also set to zero which means that a module

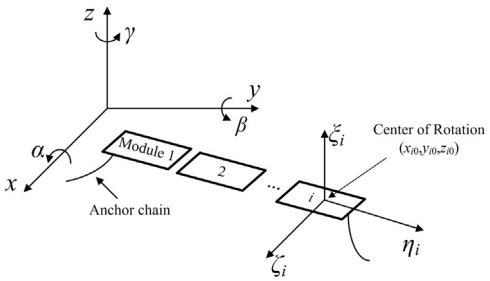

Fig. 1. Sketch of coordinate systems.

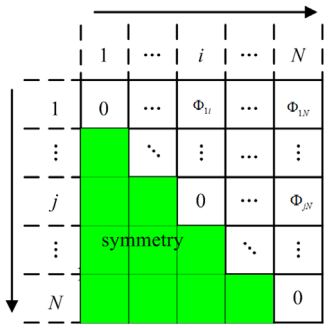

Fig. 2. Schematic diagram for the construction of connection topology matrix.

cannot connect with itself. According to the above definition for the connection topology matrix, it is easy to understand that the connection topology matrix is symmetric because of the mutual connection between the connected modules in the floating system.

Introducing the topology matrix into the dynamics model enables to deal with the arbitrary connection among the floating modules, so that the model is available to represent diverse topological VLFS by only changing the assignment of the matrix element, no matter that the floating structure is a ring form or a rectangular form or any other topological forms.

2.2. Modeling of single floating body

For a single module, by applying the linear wave theory (Stoker, 2011), we can formulate a governing equation of motion for the i-th floating module, given as

$$\mathbf{M}_i\ddot{\mathbf{X}}_i+\mathbf{C}_i\dot{\mathbf{X}}_i+\mathbf{G}(\mathbf{X}_i)=\mathbf{F}_{i,W}+\mathbf{F}_{i,C}+\mathbf{F}_{i,M}, \tag{1}$$

where $\mathbf{X}_i=[x_i,y_i,z_i,\alpha_i,\beta_i,\gamma_i]^T$ is the generalized displacement vector of the i-th module in Earth-fixed frame, where the symbols $x_i,y_i,z_i,\alpha_i,\beta_i,\gamma_i$ indicate displacement of surge, sway, heave, roll, pitch and yaw motions respectively and the superscript T denotes the transpose. For simplicity, we introduce $\mathbf{X}_{i,1}=[x_i,y_i,z_i]^T,\mathbf{X}_{i,2}=[\alpha_i,\beta_i,\gamma_i]^T$. $\mathbf{M}_i,\mathbf{C}_i$ are the mass and damping matrices of the system, $\mathbf{G}(\mathbf{X}_i)$ indicates generalized hydrostatic restoring force. The system mass matrix $\mathbf{M}_i\in\mathbb{R}^{6\times6}$ is defined as (Faltinsen, 1993)

$$\mathbf{M}_i=\begin{bmatrix} m & 0 & 0 & 0 & m(z_c-z_g) & 0\\ 0 & m & 0 & -m(z_c-z_g) & 0 & m(z_c-z_g)\\ 0 & 0 & m & 0 & -m(z_c-z_g) & 0\\ 0 & -m(z_c-z_g) & 0 & J_x & 0 & -J_{xz}\\ m(z_c-z_g) & 0 & -m(z_c-z_g) & 0 & J_y & 0\\ 0 & m(z_c-z_g) & 0 & -J_{zx} & 0 & J_z \end{bmatrix}, \tag{2}$$

where m is the floating body mass, z_g,z_c is the z coordinate of the center of gravity and rotation. J_x,J_y and J_z are the moments of inertia about the x,y and z axes and $J_{xz}=J_{zx}$ are the products of inertia. Hence, it can be shown that the system inertia matrix is symmetrical and positive definite.

$$\begin{aligned} J_x&=\iint_V(y-y_c)^2\,\mathrm{d}m+\iint_V(z-z_c)^2\,\mathrm{d}m\\ J_y&=\iint_V(z-z_c)^2\,\mathrm{d}m+\iint_V(x-x_c)^2\,\mathrm{d}m\\ J_z&=\iint_V(x-x_c)^2\,\mathrm{d}m+\iint_V(y-y_c)^2\,\mathrm{d}m, \end{aligned} \tag{3}$$

$$J_{xz}=J_{zx}=\iint_V(x-x_c)(z-z_c)\mathrm{d}m. \tag{4}$$

Here, small roll and pitch angles are assumed, such that the restoring vector $\mathbf{G}(\mathbf{X}_i)$ can be linearized to $\mathbf{S}_i\mathbf{X}_i$, where $\mathbf{S}_i\in\mathbb{R}^{6\times6}$ is a matrix of generalized linear restoring force coefficients and is written as follows for the $x-z$ plane symmetry (El-Hawary, 2002).

$$\mathbf{S}_i=-\begin{bmatrix} 0 & 0 & 0 & 0 & 0 & 0\\ 0 & 0 & 0 & 0 & 0 & 0\\ 0 & 0 & Z_z & 0 & Z_\beta & 0\\ 0 & 0 & 0 & K_\alpha & 0 & 0\\ 0 & 0 & M_z & 0 & M_\beta & 0\\ 0 & 0 & 0 & 0 & 0 & 0 \end{bmatrix}, \tag{5}$$

where the coefficients are defined as follows:

$$Z_z=-\rho gA_w, \tag{6}$$

$$Z_\beta=M_z=\rho g\iint_{A_w}x\,\mathrm{d}A, \tag{7}$$

$$K_\alpha=-\rho gV(z_b-z_g)-\rho g\iint_{A_w}y^2\,\mathrm{d}A, \tag{8}$$

$$M_\beta=-\rho gV(z_b-z_g)-\rho g\iint_{A_w}x^2\,\mathrm{d}A. \tag{9}$$

Here, g is the acceleration of gravity, z_b is the z-coordinate of the center of the buoyancy, A_w is the waterplane area, and V is the volume of the water.

Generally, the damping of system is complex and has no uniform expression. In this paper, we do not consider damping of the system thus the damping matrix $\mathbf{C}_i$ will be vanished in the following derivation.

The three terms of $\mathbf{F}_{i,W},\mathbf{F}_{i,C},\mathbf{F}_{i,M}$ in the right handside of Eq. (1) indicate the wave force, connector force and the force produced by mooring system to be derived later.

2.3. Hydrodynamic model

By assuming the water irrotational and inviscid, the linear wave theory (Stoker, 2011) is used to determine the wave force. For linear wave with regular frequency ω, the total wave potential can be expressed as $\Phi = \mathrm{Re}\left[\phi e^{-i\omega t}\right]$ where ϕ is the space velocity potential. Considering a floating system that consists of N numbers of modules separated with some gaps with no speed, the total potential can be written as

$$\phi = \phi_I + \phi_D + i\omega \sum_{i=1}^{N} \sum_{q=1}^{6} \overline{u}_i^q \phi_i^q, \tag{10}$$

where $i = \sqrt{-1}$, and ϕ_I, ϕ_D indicate incident potential and diffraction potential respectively. $\overline{u}_i^q$ is complex amplitude of the i-th module in the q-th modal, corresponding to the surge, sway, heave, roll, pitch and yaw of the module. The displacement vector of harmonic motion of the i-th module in time evolution is formulated by $\mathbf{U}_i = \overline{U}_i e^{-i\omega t}, \overline{U}_i = \left[\overline{u}_i^1, \overline{u}_i^2, \ldots, \overline{u}_i^6\right]$. ϕ_i^q is the potential due to a unit amplitude motion of the i-th module only and other modules are all fixed, referred as normalized velocity potential of the q-th modal of the i-th module.

The incident potential ϕ_I can be determined by specifying wave frequency and wave height, diffraction potential ϕ_D and normalized velocity potential ϕ_i^q satisfied Laplace equation, and conditions of free surface, body's surface boundary, sea bottom and infinity radiation, which can be written as

$$\phi_I = \frac{iga}{\omega} \frac{\cosh k(z+h)}{\cosh kh} \exp\left[ik\{x\ \cos\ \beta + y\ \sin\ \beta\}\right], \tag{11}$$

$$\begin{cases} \nabla^2 \phi_D = 0 \\ \frac{\partial \phi_D}{\partial z} - \frac{\omega^2}{g} = 0 \\ \frac{\partial \phi_D}{\partial n} = -\frac{\partial \phi_I}{\partial n} \\ \frac{\partial \phi_D}{\partial z} = 0 \quad z = -h \\ \lim\limits_{r \to \infty} \sqrt{r}\left(\frac{\partial \phi_D}{\partial r} - i\frac{\omega^2}{g}\phi_D\right) = 0 \end{cases} \qquad \begin{cases} \nabla^2 \phi_i^q = 0 \\ \frac{\partial \phi_i^q}{\partial z} - \frac{\omega^2}{g}\phi_i^q = 0 \\ \frac{\partial \phi_i^q}{\partial n}|_{S_i} = n_i^q \\ \frac{\partial \phi_i^q}{\partial n}|_{S_m} = 0 \quad (i \neq m) \\ \frac{\partial \phi_i^q}{\partial z} = 0 \quad z = -h \\ \lim\limits_{r \to \infty} \sqrt{r}\left(\frac{\partial \phi_i^q}{\partial r} - i\frac{\omega^2}{g}\phi_i^q\right) = 0 \end{cases}, \tag{12}$$

where n_i^q is the q-th modal's projection component of generalized outward normal vector of the i-th module. h indicates water depth and r represents displacement between field point and source point.

Based on the governing equation and the boundary condition, the velocity potential can be solved by using the boundary element method (in this paper, HydroD is used). After ϕ_D, ϕ_i^q are solved, the wave force can be obtained by integrating wave potential along the wet surface of the i-th module using Bernoulli' equation, we obtained

$$\begin{aligned} \overline{W}_i^p &= \iint_S \frac{\partial \phi_i^p}{\partial n} \left[-i\omega\rho \left(\phi_I + \phi_D + i\omega \sum_{j=1}^{N} \sum_{q=1}^{6} \overline{u}_j^q \phi_j^q \right) \right] \mathrm{d}s \\ &= \iint_{S_i} n_i^p \left[-i\omega\rho \left(\phi_I + \phi_D + i\omega \sum_{j=1}^{N} \sum_{q=1}^{6} \overline{u}_j^q \phi_j^q \right) \right] \mathrm{d}s. \end{aligned} \tag{13}$$

In above equation, we usually divided the wave force into two parts in which one is the wave exciting force due to the scattering potential $\phi_S = \phi_I + \phi_D$ and the other is the radiation force produced by radiation potential. They are formulated as

$$\overline{F}_{w,i}^p = -i\omega\rho \iint_S \phi_S n_i^p \, ds, \tag{14}$$

$$\overline{R}_i^p = \rho\omega^2 \left[\sum_{j=1}^{N} \sum_{q=1}^{6} \iint_{S_i} \overline{u}_j^q \phi_j^q n_i^p \, \mathrm{d}s \right] = \sum_{j=1}^{N} \sum_{q=1}^{6} \left(\omega^2 A_{ij}^{pq} + i\omega B_{ij}^{pq} \right) \overline{u}_j^q, \tag{15}$$

where

$$\begin{aligned} A_{ij}^{pq} &= \rho \iint_{S_i} \mathrm{Re}\left[\phi_j^q\right] n_i^p \, \mathrm{d}s \\ B_{ij}^{pq} &= \rho\omega \iint_{S_i} \mathrm{Im}\left[\phi_j^q\right] n_i^p \, \mathrm{d}s. \end{aligned}$$

A_{ij}^{pq}, B_{ij}^{pq} indicate added mass and added damping respectively. Considering the relationship of velocity potential, space velocity potential and normal velocity potential, Eq. (15) can be rewritten as

$$R_i^p = \overline{R}_i^p e^{-i\omega t} = \sum_{j=1}^{N} \sum_{q=1}^{6} \left(\omega^2 A_{ij}^{pq} + i\omega B_{ij}^{pq} \right) \overline{u}_j^q e^{-i\omega t} = -\sum_{j=1}^{N} \sum_{q=1}^{6} \left(A_{ij}^{pq} \ddot{u}_j^q + B_{ij}^{pq} \dot{u}_j^q \right). \tag{16}$$

For simplicity, Eqs. (14) and (16) can be written into a matrix form

$$\overline{\mathbf{F}}_{i,w} = -i\omega\rho \iint_S \phi_S \mathbf{n}_i \mathrm{d}s, \tag{17}$$

$$\mathbf{R}_i = -\sum_{j=1}^{N} \left(\mathbf{A}_{ij}\ddot{\mathbf{U}}_j + \mathbf{B}_{ij}\dot{\mathbf{U}}_j\right), \tag{18}$$

where

$$\mathbf{n}_i = \left[n_i^1, n_i^2, \ldots, n_i^6\right]^T,$$

$$\mathbf{A}_{ij} = \begin{bmatrix} A_{ij}^{11} & A_{ij}^{12} & \cdots & A_{ij}^{16} \\ A_{ij}^{21} & A_{ij}^{22} & \cdots & A_{ij}^{26} \\ \vdots & \vdots & \ddots & \vdots \\ A_{ij}^{61} & A_{ij}^{62} & \cdots & A_{ij}^{66} \end{bmatrix}.$$

According to the above derivation, when the floating modules stay in harmonic motion excited by wave force, the total wave force imposed on the i-th module can be formulated as

$$\mathbf{W}_i = \overline{\mathbf{F}}_{i,W} e^{-i\omega t} + \mathbf{R}_i. \tag{19}$$

2.4. Modeling of connectors

The position and orientation of the i-th module in the Earth-fixed frame are defined by $\mathbf{\Psi}_i = \left[\mathbf{\Psi}_{i,1}^T, \mathbf{\Psi}_{i,2}^T\right]^T$, where the first variable describes the position, while the last describes the Euler angles, there are,

$$\begin{aligned} \mathbf{\Psi}_{i,1} &= \mathbf{X}_{i0,1} + \mathbf{X}_{i,1} \\ \mathbf{\Psi}_{i,2} &= \mathbf{X}_{i,2}, \end{aligned} \tag{20}$$

where $\mathbf{X}_{i0,1} = [x_{i0}, y_{i0}, z_{i0}]^T$ is the origin position of the Body-fixed frame of the i-th module before deformation (Fig. 3).

Consider the connector p connecting the face m of module i and the face n of module j. The connection force on the face m of module i, decomposed in the Earth-fixed frame, is denoted by $\mathbf{f}_{ijmn,p}$. Clearly, the force acting on face n of module j from connector p is $\mathbf{f}_{jinm,p} = -\mathbf{f}_{ijmn,p}$. The connector p acts at the points defined by the position vectors $\mathbf{p}_{im,p}^b$ and $\mathbf{p}_{jn,p}^b$ with respect to the Body-fixed reference frames and the vectors are constant. In the global coordinate system, the position of the connection points can be described by

$$\begin{aligned} \mathbf{p}_{im,p} &= \mathbf{\Psi}_{i,1} + \mathbf{T}(\mathbf{\Psi}_i)\mathbf{p}_{im,p}^b \\ \mathbf{p}_{jn,p} &= \mathbf{\Psi}_{j,1} + \mathbf{T}(\mathbf{\Psi}_j)\mathbf{p}_{jn,p}^b, \end{aligned} \tag{21}$$

where the operator $\mathbf{T}(\bullet)$ denotes the coordinate transform matrix(Loukogeorgaki and Angelides, 2005), written as

$$\mathbf{T} = \begin{bmatrix} \cos\gamma\cos\beta & -\sin\gamma\cos\alpha + \cos\gamma\sin\beta\sin\alpha & \sin\gamma\sin\alpha + \cos\gamma\cos\alpha\sin\beta \\ \sin\gamma\cos\beta & \cos\beta\cos\alpha + \sin\alpha\sin\beta\sin\gamma & -\cos\gamma\sin\alpha + \sin\beta\sin\gamma\cos\alpha \\ -\sin\beta & \cos\beta\sin\alpha & \cos\beta\cos\alpha \end{bmatrix}. \tag{22}$$

The vector describing the relative position of two connecting points is given as

$$\mathbf{l}_{ijmn,p} = \mathbf{p}_{jn,p} - \mathbf{p}_{im,p}, \tag{23}$$

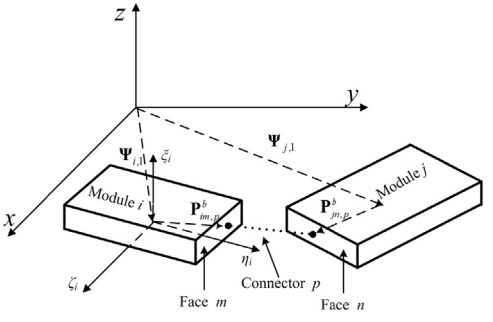

Fig. 3. Sketch for the position relationship between adjacent modules and connector.

while the distance between the connection points is given by

$$l_{ijmn,p} = \|\mathbf{p}_{jn,p} - \mathbf{p}_{im,p}\|. \tag{24}$$

The connector will impose forces on the modules at $\mathbf{p}_{im,p}$ and $\mathbf{p}_{jn,p}$, as well as their torques at the gravity center of the modules.

The direction vector for the projection of the connector deformation is formulated as

$$\mathbf{n}_{ijmn} = \frac{\mathbf{l}_{ijmn,p}}{l_{ijmn,p}}. \tag{25}$$

The translational restoring forces along the connectors are derived from Eqs. (23) and (25) written as

$$\mathbf{f}_{ijmn,p} = (l_{ijmn,p} - \delta_p)\mathbf{n}_{ijmn}, \tag{26}$$

where the symbol δ_p indicates the initial length of the connector p, which can be calculated by the distance formula before deformation, written as

$$\delta_p = \|\mathbf{p}_{jn0,p} - \mathbf{p}_{im0,p}\| = \|\left(\mathbf{X}_{j0,1} + \mathbf{p}^b_{jn0,p}\right) - \left(\mathbf{X}_{i0,1} + \mathbf{p}^b_{im0,p}\right)\|. \tag{27}$$

The vector of the arm of force imposed on the rotation center of the i-th module due to connector forces in the Earth-fixed reference are formulated as

$$\mathbf{r}_{ijm,p} = \mathbf{p}_{im,p} - \mathbf{\Psi}_{i,1}. \tag{28}$$

The force acting on the module will induce torques about the gravity center of modules. The torque vector in the Earth-fixed reference frame is formulated as

$$\mathbf{m}_{ijmn,p} = \mathbf{r}_{ijm,p} \times \mathbf{f}_{ijmn,p}. \tag{29}$$

For a multi-module floating structure, usually a module may connect with adjacent modules via several faces or only one face. To be able to deal with arbitrary connection, we need to number all faces of modules in the sense of local numbering on individual module and global numbering based on the entire floating structure . Fig. 4 illustrates an example for the face numbering of two connected triangle modules. There are module I and module J, and their faces are represented by the triangle side lines. The local faces of module I are numbered by I_1, I_2, and I_3, and the local faces of module J are numbered by J_1, J_2, and J_3. The global numbering is denoted by 1,2,3,… on all the faces of the two modules. Each local face number corresponds to a global face number. There is a rule for the global numbering. If the face I_i of the module I is connected with the face J_j of module J, the same global number should be assigned to both the faces. Taking an example in Fig. 4, the connected faces of local face numbers are I_3 and J_1, shown in thick lines. The global face number for both the faces should be given by number 5.

The global and local face numbers are tabulated in Table 1, where the two modules are connected only via the global face number 5.

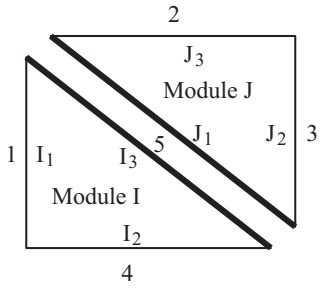

Fig. 4. Face numbering for connected modules. I_i and J_j are the local face numbering, and 1,2,3,4,5 are the global face numbering. The connected faces between module I and J share the same global number 5.

Table 1
Local and global face numbers for the example of Fig. 4.

Module	I			J		
Local face number	I_1	I_2	I_3	J_1	J_2	J_3
Global face number	1	4	**5**	**5**	3	2

Let symbol $\Gamma(\bullet)$ denote a series of the global face numbers. If the global face number $\Gamma(m)$ is identical to $\Gamma(n)$, the face connection index Ξ_{mn} is assigned by a value of 1, otherwise 0, written as

$$\Xi_{mn} = \begin{cases} 1 & \Gamma(m) = \Gamma(n) \\ 0 & \Gamma(m) \neq \Gamma(n) \end{cases}. \tag{30}$$

In Eq. (30) the face connection index defines which face of a module is connected with which face of other module.

Since a module should not be connected by itself, there is $\mathbf{f}_{iimm,p} = 0$. The connection force imposed on module i in the Earth-fixed reference frame due to the connection with module j can be formulated as

$$\mathbf{F}_{ij}^{c} = \sum_{p=1}^{N_c} \Xi_{mn} k_p \begin{bmatrix} \mathbf{f}_{ijmn,p} \\ \mathbf{m}_{ijmn,p} \end{bmatrix}, \tag{31}$$

where N_c is the number of the connectors between the module i and j.

If all the connectors have the same stiffness k_c, that is

$$k_p = k_c, \quad p = 1, 2, \ldots, N_c \tag{32}$$

then the connection force imposed on module i in the Earth-fixed reference frame due to the connection with module j is

$$\mathbf{F}_{ij}^{c} = k_c \sum_{p=1}^{N_c} \Xi_{mn} \begin{bmatrix} \mathbf{f}_{ijmn,p} \\ \mathbf{m}_{ijmn,p} \end{bmatrix}. \tag{33}$$

Eq. (31) is a constitutive model for the connectors with stiffness k_p, which describe force–deformation relationship of connectors. The derivation process of the model becomes easy when introducing two sets of coordinates and using coordinate transformation. The model (33) is simple. It only needs the information of the coordinates of connection points in the local body coordinate, and generally suitable for any type of topological connections, while the previous work (Zhang et al., 2015a) has to involve repeatedly complex mathematic derivation of the model for a particular type of connection. Note that the model of the connectors contains nonlinear geometric characteristics and the coupling terms of module response vector. It indicates that the stiffness of the connection between adjacent modules in a specified degree of freedom depends on the motions in other degrees of freedom even if the elasticity of a single connector possesses a linear property. In addition, the nonlinearity could be very strong because the small motion of modules may cause large deflection at connection points due to huge differences of the size scale between modules and connectors.

2.5. Network model of multi-module floating structures

For the network model of multi-module floating structure with arbitrary topology, its governing equations can be formulated as follows step by step.

For the wave force imposed on each module, Eq. (19) can precisely calculate the total wave force if the harmonic motion of a module coincides with the wave frequency. For nonlinear dynamic system, strictly speaking, the wave force should be integrated at each time step because the nonlinear responses may not be a harmonic motion, so that the computation becomes highly costly. Considering nonlinear responses are mostly dominated by the fundamental frequency in frequency spectrum, we adopt an approximate approach by taking $\mathbf{X}_i \approx \mathbf{U}_i$, such that the wave force can be formulated as

$$\mathbf{F}_{i,W} \doteq \mathbf{W}_i = \overline{\mathbf{F}}_{i,W} e^{-i\omega t} - \sum_{j=1}^{N} \left(\mathbf{A}_{ij} \ddot{\mathbf{X}}_j + \mathbf{B}_{ij} \dot{\mathbf{X}}_j \right). \tag{34}$$

In order to deal with arbitrary topology types of floating structures, a topology matrix $\Phi \in \mathbb{R}^{N \times N}$ is introduced where its element Φ_{ij} is set to 1 when the i-th module connects with the j-th module, otherwise Φ_{ij} is set to zero. Considering the possible connection couplings of all modules, the total connector force imposed on the i-th module can be described as

$$\mathbf{F}_{i,C} = \varepsilon \sum_{j=1}^{N} \Phi_{ij} G(\mathbf{X}_i, \mathbf{X}_j), \tag{35}$$

where ε is the coupling strength, physically representing the stiffness of connectors. $G(\mathbf{X}_i, \mathbf{X}_j)$ is the coupling function which defines the specific interaction in different degrees of freedom between the i-th module and the j-th module. In this model it represents the constitutive relationship of the connector in Eq. (33), expressed by

$$G(\mathbf{X}_i, \mathbf{X}_j) = \sum_{p=1}^{N_c} \Xi_{mn} \begin{bmatrix} \mathbf{f}_{ijmn,p} \\ \mathbf{m}_{ijmn,p} \end{bmatrix}. \tag{36}$$

The floating structure may be practically constrained by a mooring system to prevent drifting. Considering the simplest linear mooring model, the mooring force imposed on the i-th module can be written as

$$\mathbf{F}_{i,M} = -\delta(i, i_0) \mathbf{K}_i \mathbf{X}_i, \tag{37}$$

where i_0 is the number of the module which mooring system acts. $\delta(i,i_0)$ denotes Delta function which is satisfied

$$\delta(i,i_0)=\begin{cases}0, & i\neq i_0\\ 1, & i=i_0\end{cases}. \tag{38}$$

A network model of multi-module floating structure can be formed based on the single module governing Eq. (1), the total wave force expression (34), the constitutive model of connector (35) and the constraint model of mooring system. The governing equations for an N-module floating structure can be generally written as

$$\mathbf{M}_i\ddot{\mathbf{X}}_i+\sum_{j=1}^{N}\left(\mathbf{A}_{ij}\ddot{\mathbf{X}}_i+\mathbf{B}_{ij}\dot{\mathbf{X}}_i\right)+[\mathbf{S}_i+\delta(i,i_0)\mathbf{K}_i]\mathbf{X}_i=\mathbf{F}_{i,w}e^{-i\omega t}+\varepsilon\sum_{j=1}^{N}\Phi_{ij}G(\mathbf{X}_i,\mathbf{X}_j),\quad i=1,\ldots,N. \tag{39}$$

By now, a generalized three-dimensional network model (39) for a multi-module floating structure is developed which is available to any type of connectors in arbitrary topology structures. When tailoring to a particular model for computation, we should first define the topological matrix according to the design of structure topology, assigning the numbers for the modules and connectors, and then connection faces of connectors.

3. Numerical illustrations for a multi-module floating airport

For the illustration of the feasibility of modeling method, a floating airport is considered which is connected by five modules in a chain-type of structure topology.

3.1. Parameters of simulating model

A floating airport is constructed by serially connecting five identical semi-submersible floating modules in waves. The configuration sketch and the assignment of the numbers of modules and connectors are shown in Fig. 5.

In Fig. 5, M1–M5 indicate the modules and the blue lines labeled with C_1–C_8 denote the connectors. Each module is symmetric with respect to plants of $O_i\zeta_i\xi_i$ and $O_i\eta_i\xi_i$. The pertinent information of a single module is given in Table 2. The connection points are arranged at upper hull and their coordinates in the body-fixed frame are $(\pm 150, \pm 40, 12)$. The initial length of the connector and the gap between adjacent modules is $\delta=25\ m$.

For the chain-type floating airport with the module number shown in Fig. 5, the topology matrix Φ can be formulated as

$$\Phi_{ij}=\begin{cases}1 & j=i+1\\ 0 & others\end{cases}\quad i=1,2,\ldots,5;\quad j=i,i+1,\ldots,5. \tag{40}$$

We can see that the topology matrix in Eq. (40) is a diagonal matrix. For the chain-type floating airport, face number is illustrated in Fig. 6. The blue color numbers indicate local face numbers and black numbers indicate global face numbers.

In order to constrain a drift of the floating airport, module-1 and module-5 are constrained by anchor chains. So the effect of constrained boundary condition is represented by the linear mooring stiffness matrix in which the stiffness coefficients in each degree of freedom are assigned as $K_{ii}=1\times 10^8 N/m$ $(i=1,\ldots,6)$.

For the wave parameters, the wave frequency is spanned in the interval of $0.1-1.5\mathrm{rad}/s$. The wave height is set at $a=5\ m$ and water depth is set at $h=300\ m$. The works (Riggs et al., 2000, 1998a, 1998b; Wu and Mills, 1996) revealed that the most dangerous work condition happens approximately at 85° wave angle, so we only choose this scenario for the numerical simulation for the illustration purpose.

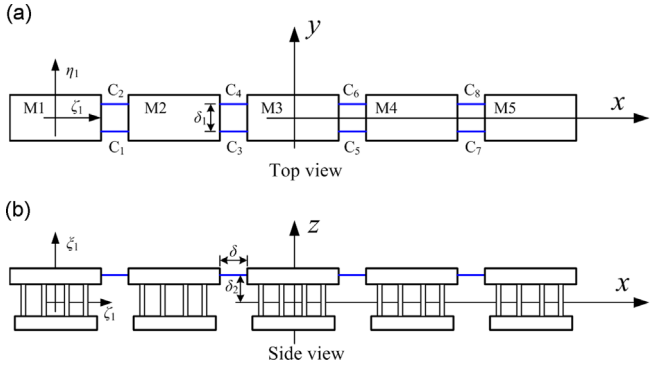

Fig. 5. Configuration sketch of 5-module floating airport.

Table 2
Principal characteristics of a single module.

Term	Parameter (Unit)	Value
Upper hull	Length (m)	300
	Breadth (m)	100
	Depth (m)	6
Columns	Length (m)	16
	Diameter (m)	18
	Transverse spacing (m)	58
	Longitudinal spacing (m)	60
Lower hull	Length (m)	270
	Breadth (m)	27
	Depth (m)	5
Others	Vertical height of gravity center (m)	12
	Design draft (m)	12
	Displacement (t)	93 614
	Moment of inertia for x, y, z axis (kg m^2)	1.089×10^{11}
		7.282×10^{11}
		7.282×10^{11}

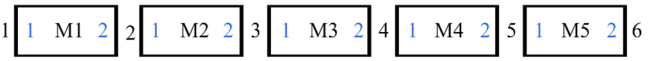

Fig. 6. Sketch for face numbering of 5-module floating airport. (For interpretation of the references to color in this figure legend, the reader is referred to the web version of this article.).

3.2. Nonlinear dynamic response and connector load

Most existing research works on VLFS do not consider the effect of nonlinear dynamics. In order to explain the necessity of considering nonlinearity, we will purposely add the linear results for the comparison with nonlinear case. When linearizing the nonlinear coupling function G, it yields,

$$G_L(\mathbf{X}_i, \mathbf{X}_j) = K_L(\mathbf{X}_j - \mathbf{X}_i), \tag{41}$$

where linearized coupling matrix K_L can be formulated as

$$K_L = \begin{bmatrix} 2 & 0 & 0 & 0 & 2\delta_2 & 0 \\ 0 & 0 & 0 & 0 & 0 & 0 \\ 0 & 0 & 0 & 0 & 0 & 0 \\ 0 & 0 & 0 & 0 & 0 & 0 \\ 2\delta_2 & 0 & 0 & 0 & {\delta_2}^2 & 0 \\ 0 & 0 & 0 & 0 & 0 & {\delta_1}^2/2 \end{bmatrix}, \tag{42}$$

where δ_1 is the horizontal distance between two parallel connectors and δ_2 is the vertical distance between the connectors and free water surface which is marked in Fig. 5. It is easy to find that the linearized coupling matrix K_L is almost decoupling except surge and pitch motions, and in sway, heave and roll, the linearized model has no coupling effect because of ignoring high order terms of coupling function.

In order to understand the coupling characteristics of the connector in the case of nonlinearity, the six components of the coupling function G versus only two relative displacements of the surge motion Δx and roll motion $\Delta\alpha$ while other displacements are all set with zero which is shown in Fig. 7.

The surge motion (shown in Fig. 7(a)) and pitch motion (shown in Fig. 7(e)) almost only depend on the relative surge motion Δx but the other four motions components of G function have strong nonlinear relationship with the two relative displacements of surge and roll motions. When examining the four components discussed above clearly in Fig. 7, it is easy to find that they all appear as curvature surfaces in the three dimensional space which implies that they have nonlinear characteristics. Note that Fig. 7 only illustrates the effect of two relative displacements. In fact, a connector force in a certain degree of freedom may be seriously affected by the motions of all other degrees of freedom. While linearization methods assume connector forces independent in each degree of freedom, ignoring the coupling effect of nonlinearity, it may result in unreasonable results.

To understand the effect of the geometric nonlinearity of connectors on dynamic response, Fig. 8 illustrates the system response versus connector stiffness in wave frequency $\omega = 0.5$. The heave motions of five modules versus connector stiffness are shown in Fig. 8(a). For small connector stiffness in the interval of $2.2 \times 10^6 < k_c < 8.4 \times 10^8$, the nonlinear responses

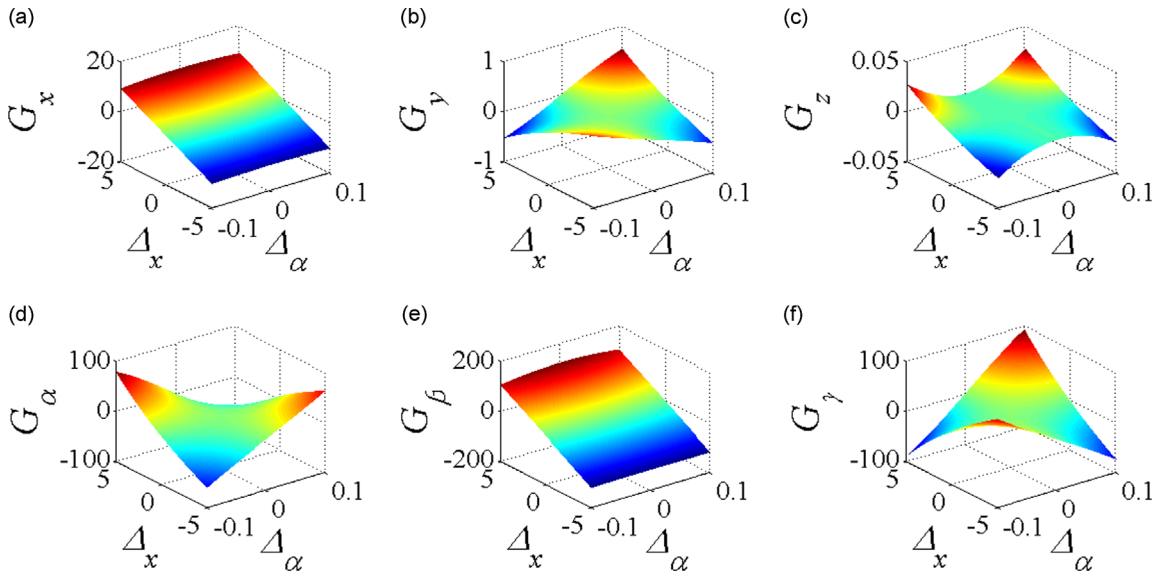

Fig. 7. Nonlinear coupling function G against relative displacement Δ_x and Δ_α.

denoted by broken lines show that the motion pattern is chaotic or sub-harmonic oscillation. With the increase of connector stiffness, the response curves appear smooth associating with a simple harmonic motion. The amplitude of motions in chaotic or sub-harmonic region is always larger than that of the simple harmonic region. Note that every module has the same oscillation pattern, which means that all modules behave similarly under the same parameters settings although their amplitudes could have discrepancy. In other words, if one module settles in a chaotic state the others will settle to the same pattern as well. It is worthy to remark that such synchronous phenomena also happen among different degrees of freedom, although not shown here. In order to see the differences between linear and nonlinear results, we chose module M2 as an example. Fig. 8(b) shows the amplitude of surge motion for module M2 versus connector stiffness both for the nonlinear and linear responses. In general, the nonlinear amplitude is much larger than the linear result, and the maximum amplitude of the nonlinear response is doubled over the linear one. Linear resonance (solid line) happens narrowly while the nonlinear resonance covers much larger region. From Fig. 8(c) to (g), the figures show the roll, sway and heave motions and so on. The nonlinear response curves almost have the same pattern as the surge motion in Fig. 8(b); however, the linear responses are almost constant with the increase of connector stiffness. When we examine the linearized model, we find that the change of the stiffness of the horizontal placed connectors can only take effect on the surge motion but cannot influence the stiffness in the roll, sway and heave directions, because the linearization process truncates the effects of high order terms in the nonlinear constitutive model of the connector. For the pith motion of module M2 shown in Fig. 8(e), the linear and nonlinear results also have resonance region like surge motion shown in Fig. 8(b), but the amplitude for the nonlinear result is still larger. Fig. 8(g) illustrates the yaw motion of module M2. The nonlinear result is about the same in comparison with the linear response at the peak of resonance of $k_c = 2.13 \times 10^8$, apart from which the nonlinear results are much larger than linear results. We can conclude that nonlinear responses in general are much larger than the linear one, and the fierce oscillations also cover wider parameter region. In another words, the linearization method may underestimate the actual response level of the floating structure.

Considering the wave condition may change over the time, we are interested in the variation of module responses when the wave frequency changes. Taking an example by choosing a typical stiffness $k_c = 2.13 \times 10^8$ at the resonance of the yaw motion, referring to Fig. 8(g), the variation of the nonlinear responses is shown in Fig. 9.

For the surge motion (shown in Fig. 9(a)) and pitch motion (shown in Fig. 9(d)), it is easy to find that the wave frequency plays a great role in nonlinear results and there are some resonance peaks in the frequency interval we chose, but the linear results have minor changes. For the wave angle we choose in this case, we know that, no matter what wave frequencies, the wave force imposed in these two directions is weak. So the results of linearized model are always very small in the wave frequency domain. For nonlinear case, however, the motions in these two directions are coupled with others, so that the oscillation energy can transfer among these motions. Fig. 9(b) illustrates the roll motion of module M2. The nonlinear amplitude is much larger than the linear results in low frequency band while there is tiny discrepancy in the region of high frequency band. From Fig. 9(c), the nonlinear and linear variation trends for sway freedom are similar, but linear results appear to a smooth curve while nonlinear results have a number of peaks. The reason for these peaks is that the system responses involve chaotic or high-order motion patterns in nonlinear model. Fig. 9(e) illustrates the amplitude–frequency curves of heave motion. The trend of the response curve of the linear result coincides well with nonlinear result, but the peak value of the nonlinear result is more than twice compared with linear results. For the yaw motion shown in Fig. 9(f), there is a large discrepancy between the linear and nonlinear results in low frequency band, similar to the surge and pitch

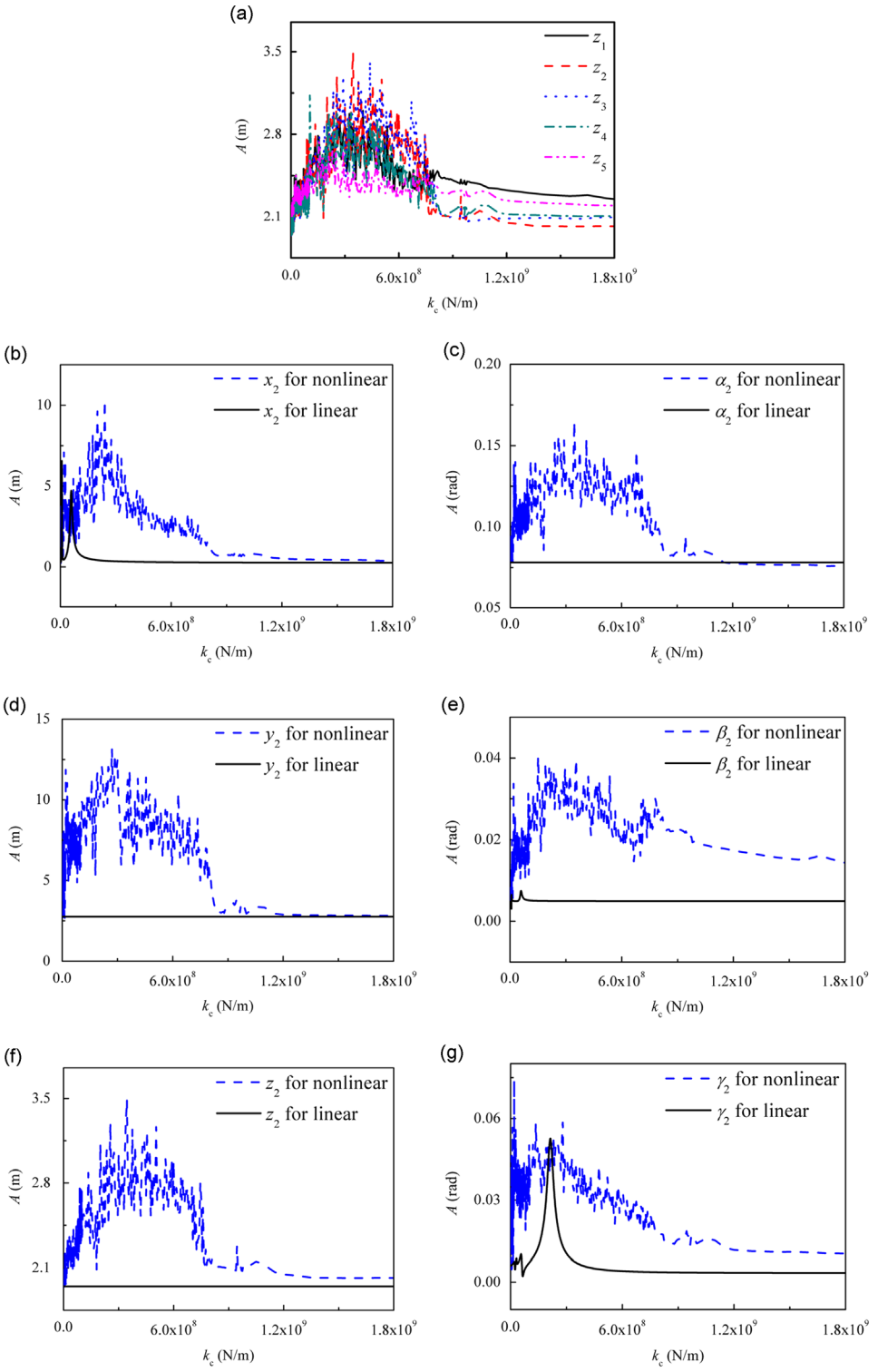

Fig. 8. The response amplitude versus connector stiffness for wave angle $\psi = 85^{\circ}$, wave height $a = 5\ m$, and wave frequency $\omega = 0.5\mathrm{rad}/s$.

motions. When we examine the middle section of frequency band, the peaks of the linear and nonlinear curves are located in different positions but close, which may be caused by a inclined resonance peak of nonlinear system (Zhang et al., 2015a).

Connector is a key element for the multi-module floating structures, and the connector load under various module motions is seriously concerned. Fig. 10 illustrates the connector load under changes in connector stiffness and wave

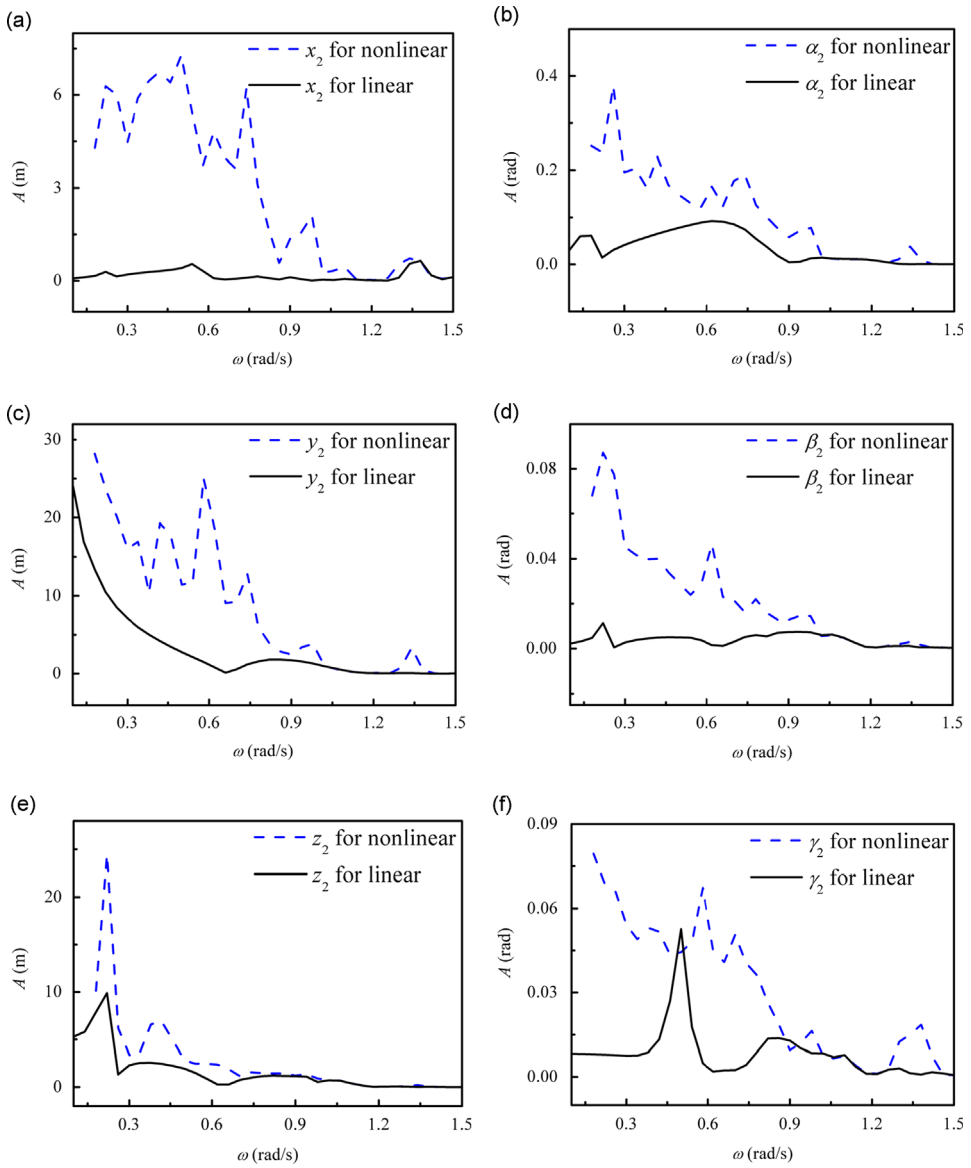

Fig. 9. Amplitude–frequency curves for wave angle $\psi = 85^{\circ}$, wave height $a = 5\ m$ and connector stiffness $k_c = 2.13 \times 10^8\ N/m$.

frequency. Fig. 10(a) shows the connector load versus connector stiffness for wave frequency $\omega = 0.5 \mathrm{rad}/s$. For linear results, there are two dominant resonance peaks at connector stiffness $k_c = 5.8 \times 10^7$, $k_c = 2.13 \times 10^8$ which coincide well with the resonance peaks of surge and yaw motions. Similar to response curves, connector load also has a wide resonance region. For the maximum connector load, the nonlinear result is 1.6 times more than the linear result. Fig. 10(b) illustrates the connector load versus wave frequency for connector stiffness $k_c = 2.13 \times 10^8\ N/m$. The evolution of nonlinear connector load is similar to the surge motion in Fig. 9(a) and the connector load is always large in low frequency region. But for linear result, there is only a dominant resonance peak in middle frequency band which coincides with the yaw resonance peak. In comparison with the maximum connector load between linear and nonlinear results, there is a discrepancy over two times.

According to the above numerical analysis, we could conclude that the nonlinear response and connector load are much larger than linear results. The coupling effect in nonlinear network structure can play a significant role in the results of the response and connector load. The decoupling treatment of linearization methods might underestimate the module responses and connector loads, leading to unrealistic optimistic design results. Nevertheless, we have to note that only the numerical simulation still cannot draw a convinced conclusion which needs to be experimentally verified in our future work.

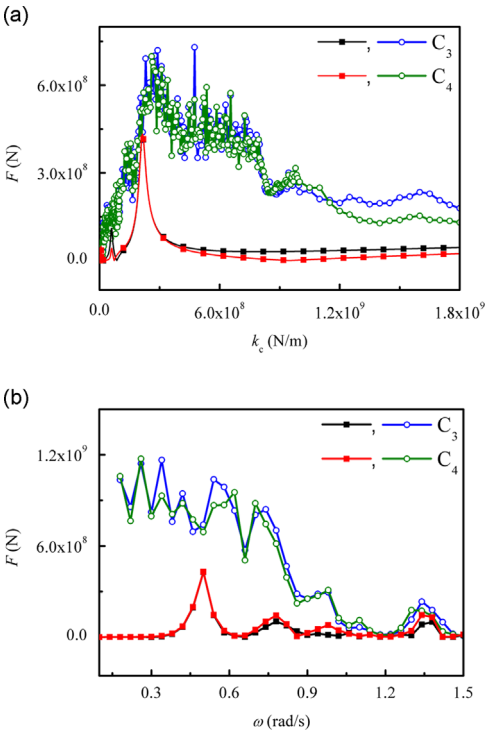

Fig. 10. Connector load variation in changes of (a) connector stiffness at wave frequency $\omega = 0.5\text{rad/s}$; (b) wave frequency at stiffness $k_c = 2.13 \times 10^8 N/m$ (for wave angle $\psi = 85^{\circ}$, wave height $a = 5$ m, diamond line for linear results, circular line for nonlinear results).

4. Conclusions

In this paper, a network modeling method is introduced to model the multi-module floating structures of arbitrary topological form. A generalized three-dimensional network model is developed based on linear hydrodynamic model, model of flexible connector with geometric nonlinearity and constraint model of mooring system. The modeling method is suitable for any type of connection configurations by only defining a structure topology matrix and connection face index. A numerical example for chain-type multi-module floating airport is illustrated to verify the feasibility of its applications. The nonlinear dynamic response and connector load are simulated in the connection stiffness and wave frequency domains together with the comparison of the linear counterpart. Numerical results show that the nonlinear results are in general larger than linear results. Although we only present the nonlinear results in particular parameters without extreme sea conditions, the analysis results can lead to a general conclusion that the coupling effect in nonlinear model cannot be simply ignored. The generalized model derived in this paper can be applied to various engineering problems with network structures alike.

Acknowledgments

This research work was supported by the 973 research Grant (2013CB036104), the National Natural Science Foundation of China (11472100) and the Graduate Student Research Innovation Project of Hunan Province (CX2015B085).

References

Andrianov, A.I., Hermans, A.J., 2005. Hydroelasticity of a circular plate on water of finite or infinite depth. Journal of Fluids and Structures 20, 719–733, http://dx.doi.org/10.1016/j.jfluidstructs.2005.03.002.

Aoki, S., 1997. Shallow water effect on hydrodynamic coefficients of very large floating structures. In: Proceedings of 7th International Offshore Polar Engineering Conference, pp. 253–260.

Du, S.X., Ertekin, C.R., 1991. Dynamic response analysis of a flexibly joined, multi-module very large floating structure. In: OCEANS 91 Proceedings. IEEE, pp. 1286–1293. doi: 10.1109/OCEANS.1991.606474.

El-Hawary, F., 2002. The Ocean Engineering Handbook. CRC Press.

Faltinsen, O., 1993. Sea Loads on Ships and Offshore Structures. Cambridge University Press.

Fu, S.X., Moan, T., Chen, X.J., Cui, W.C., 2007. Hydroelastic analysis of flexible floating interconnected structures. Ocean Engineering 34, 1516–1531, http://dx.doi.org/10.1016/j.oceaneng.2007.01.003.

Gao, R.P., Tay, Z.Y., Wang, C.M., Koh, C.G., 2011. Hydroelastic response of very large floating structure with a flexible line connection. Ocean Engineering 38, 1957–1966, http://dx.doi.org/10.1016/j.oceaneng.2011.09.021.
Hamamoto, T., 1994. Dynamic response of flexible circular floating islands subjected to stochastic waves. In: Proceedings of International Conference Hydro-Elasticity Marine Technology, pp. 433–445.
June Bai, K., Suk Yoo, B., Whan Kim, J., 2001. A localized finite-element analysis of a floating runway in a harbor. Marine Structures 14, 89–102, http://dx.doi.org/10.1016/S0951-8339(00)00030-7.
Kashiwagi, M., 1998. A B-spline Galerkin scheme for calculating the hydroelastic response of a very large floating structure in waves. Journal of Marine Science and Technology 3, 37–49, http://dx.doi.org/10.1007/BF01239805.
Khabakhpasheva, T.I., Korobkin, A.A., 2001. Reduction of hydroelastic response of floating platform in waves. In: Proceedings of 16th Internationall WkspWater Waves Floating Bodies. Hiroshima, Japan, pp. 73–76.
Khabakhpasheva, T.I., Korobkin, A.A., 2002. Hydroelastic behaviour of compound floating plate in waves. Journal of Engineering Mathematics 44, 21–40, http://dx.doi.org/10.1023/A:1020592414338.
Kim, D., Chen, L., Blaszkowski, Z., 1999. Linear frequency domain hydroelastic analysis for McDermott's mobile offshore base using WAMIT. In: Proceedings of The Third International Workshop on Very Large Floating Structures, VLFS, pp. 105–113.
Koh, H.S., Lim, Y.B., 2009. The floating platform at the Marina Bay, Singapore. Structural Engineering International 19, 33–37. 10.2749/101686609787398263.
Lee, C.H., Newman, J.N., 2000. An assessment of hydroelasticity for very large hinged vessels. Journal of Fluids and Structures 14, 957–970, http://dx.doi.org/10.1006/jfls.2000.0305.
Loukogeorgaki, E., Angelides, D.C., 2005. Stiffness of mooring lines and performance of floating breakwater in three dimensions. Applied Ocean Research 27, 187–208, http://dx.doi.org/10.1016/j.apor.2005.12.002.
Maeda, H., Maruyama, S., Inoue, R., Watanabe, K., Togawa, S., Suzuki, F., 1979. On the motions of a floating structure which consists of two or three blocks with rigid or pin joints. Journal of the Society of Naval Architects of Japan 1979, 71–78, http://dx.doi.org/10.2534/jjasnaoe1968.1979.71.
Michailides, C., Loukogeorgaki, E., Angelides, D.C., 2013. Response analysis and optimum configuration of a modular floating structure with flexible connectors. Applied Ocean Research 43, 112–130, http://dx.doi.org/10.1016/j.apor.2013.07.007.
Park, S.-W., Lee, T.-K., Hong, S.Y., 2004. A study of preliminary structural design of pontoon type VLFS. In: The Fourteenth International Offshore and Polar Engineering Conference. International Society of Offshore and Polar Engineers. Toulon, France, pp. 630–636.
Paulling, J.R., Tyagi, S., 1993. Multi-module floating ocean structures. Marine Structures 6, 187–205, http://dx.doi.org/10.1016/0951-8339(93)90019-Y.
Price, W.G., Wu, Y., 1986. Hydroelasticity of Marine Structures. Elsevier Science Publishers.
Riggs, H.R., Ertekin, R.C., 1993. Approximate methods for dynamic response of multi-module floating structures. Marine Structures 6, 117–141, http://dx.doi.org/10.1016/0951-8339(93)90016-V.
Riggs, H.R., Ertekin, R.C., Mills, T.R.J., 1998a. Impact of connector stiffness on the response of a multi-module mobile offshore base. In: The Eighth International Offshore and Polar Engineering Conference. International Society of Offshore and Polar Engineers, pp. 126–133.
Riggs, H.R., Ertekin, R.C., Mills, T.R.J., 1998b. Wave-induced response of a 5-module mobile offshore base. In: Proceedings of the17th International Conference on Offshore Mechanics and Arctic Engineering. Lisbon, pp. OMAE98–4440.
Riggs, H.R., Ertekin, R.C., Mills, T.R.J., 2000. A comparative study of RMFC and FEA models for the wave-induced response of a MOB. Marine Structures 13, 217–232, http://dx.doi.org/10.1016/S0951-8339(00)00029-0.
Rognaas, G., Xu, J., Lindseth, S., Rosendahl, F., 2001. Mobile offshore base concepts. Concrete hull and steel topsides. Marine Structures 14, 5–23, http://dx.doi.org/10.1016/S0951-8339(00)00019-8.
Stoker, J.J., 2011. Water Waves: The Mathematical Theory with Applications. Wiley-Interscience.
Utsunomiya, T., Moan, T., Watanabe, E., Wang, C.M., 2004. Very Large Floating Structures: Applications, Analysis and Design. Singapore.
Wang, C.M., Riyansyah, M., Choo, Y.S., 2009. Reducing hydroelastic response of interconnected floating beams using semi-rigid connections. In: ASME 2009 28th International Conference on Ocean, Offshore and Arctic Engineering. American Society of Mechanical Engineers, pp. 1419–1425. 10.1115/OMAE2009-79692.
Wang, D., Ertekin, R.C., Riggs, H.R., 1991. Three-dimensional hydroelastic response of a very large floating structure. International Journal of Offshore and Polar Engineering. 1, 307–316.
Watanabe, E., Utsunomiya, T., Wang, C.M., 2004. Hydroelastic analysis of pontoon-type VLFS: a literature survey. Engineering Structures 26, 245–256, http://dx.doi.org/10.1016/j.engstruct.2003.10.001.
Watanabe, E., Utsunomiya, T., Wang, C.M., Hang, L.T.T., 2006. Benchmark hydroelastic responses of a circular VLFS under wave action. Engineering Structures 28, 423–430, http://dx.doi.org/10.1016/j.engstruct.2005.08.014.
Wu, C., Mills, T.R.J., 1996. Wave-induced connector loads and connector design considerations for the mobile offshore base. In: Proceedings of International Workshop on Very Large Floating Structures. pp. 387–392.
Xia, D., Kim, J.W., Ertekin, R.C., 2000. On the hydroelastic behavior of two-dimensional articulated plates. Marine Structures 13, 261–278, http://dx.doi.org/10.1016/S0951-8339(00)00028-9.
Xu, D.L., Zhang, H.C., Lu, C., Qi, E.R., Hu, J.J., Wu, Y.S., 2014a. On Study of Nonlinear Network Dynamics of Flexibly Connected Multi-Module Very Large Floating Structures, in: Vulnerability, Uncertainty, and Risk. American Society of Civil Engineers, Reston, VA1805–1814, http://dx.doi.org/10.1061/9780784413609.181.
Xu, D.L., Zhang, H.C., Lu, C., Qi, E.R., Tian, C., Wu, Y.S., 2014b. Analytical criterion for amplitude death in nonautonomous systems with piecewise nonlinear coupling. Physical Reviews E 89, 42906, http://dx.doi.org/10.1103/PhysRevE.89.042906.
Zhang, H.C., Xu, D.L., Lu, C., Qi, E.R., Hu, J.J., Wu, Y.S., 2015a. Amplitude death of a multi-module floating airport. Nonlinear Dynamics 79, 2385–2394, http://dx.doi.org/10.1007/s11071-014-1819-x.
Zhang, H.C., Xu, D.L., Lu, C., Xia, S.Y., Qi, E.R., Hu, J.J., Wu, Y.S., 2015b. Network dynamic stability of floating airport based on amplitude death. Ocean Engineering 104, 129–139, http://dx.doi.org/10.1016/j.oceaneng.2015.05.008.